Carbonation by fluid-rock interactions at high-pressure conditions: Implications for carbon cycling in subduction zones

Carbonation by fluid-rock interactions at high-pressure conditions: Implications for carbon cycling in subduction zones

Autori: Piccoli F; Vitale Brovarone A; Beyssac O; Martinez I; Ague JJ; Chaduteau C

EARTH AND PLANETARY SCIENCE LETTERS 445 (2016) p. 146-159

Digital Object Identifier 10.1016/j.epsl.2016.03.045

Keywords

subduction carbon cycle; carbonation; CO2 sequestration; metasomatism

Abstract

Carbonate-bearing lithologies are the main carbon carrier into subduction zones. Their evolution during metamorphism largely controls the fate of carbon, regulating its fluxes between shallow and deep reservoirs. Recent estimates predict that almost all subducted carbon is transferred into the crust and lithospheric mantle during subduction metamorphism via decarbonation and dissolution reactions at high-pressure conditions. Here we report the occurrence of eclogite-facies marbles associated with metasomatic systems in Alpine Corsica (France). The occurrence of these marbles along major fluid-conduits as well as textural, geochemical and isotopic data indicating fluid–mineral reactions are compelling evidence for the precipitation of these carbonate-rich assemblages from carbonic fluids during metamorphism. The discovery of metasomatic marbles brings new insights into the fate of carbonic fluids formed in subducting slabs. We infer that rock carbonation can occur at high-pressure conditions by either vein-injection or chemical replacement mechanisms. This indicates that carbonic fluids produced by decarbonation reactions and carbonate dissolution may not be directly transferred to the mantle wedge, but can interact with slab and mantle-forming rocks. Rock-carbonation by fluid–rock interactions may have an important impact on the residence time of carbon and oxygen in subduction zones and lithospheric mantle reservoirs as well as carbonate isotopic signatures in subduction zones. Furthermore, carbonation may modulate the emission of CO2 at volcanic arcs over geological time scales.

1. Introduction

Subduction exerts a key role in the long-term carbon cycle by regulating the fluxes of carbon between the Earth's surface and the deep Earth. The redistribution of carbon between the exogenic and endogenic reservoirs largely depends on the evolution of carbonate-bearing lithologies in subduction zones. Carbonates are present in sedimentary, mafic and ultramafic lithologies, and constitute the dominant reservoir of carbon in the subducting lithosphere (Alt and Teagle, 1999, Kelemen and Manning, 2015). There is growing evidence that carbonates can be extremely reactive during subduction metamorphism via devolatilization reactions (Cook-Kollars et al., 2014, Kerrick and Connolly, 2001), as well as carbonate dissolution via fluid–rock interactions at high-pressure conditions (Frezzotti et al., 2011, Ague and Nicolescu, 2014, Kelemen and Manning, 2015), carbonate reduction reactions (Galvez et al., 2013a, Malvoisin et al., 2012), or melting of the subducting crust (Poli, 2015). Nonetheless, key questions remain regarding the mechanisms of carbonic fluid transfer from the slab to the lithospheric mantle in the sub-arc region, their role in mantle wedge metasomatism, and their contribution to the CO2 degassing at volcanic arcs.

To address these questions, a growing number of studies have been carried out using both experimental petrology (Molina and Poli, 2000, Poli et al., 2009) and thermodynamic modeling (Kerrick and Connolly, 2001, Gorman et al., 2006). All these studies agree that, considering a “closed system” (no external fluid supply), significant carbon transfer to the mantle wedge is feasible only at shallow depth in the forearc region. This

transfer is made possible via devolatilization reactions that, based on experimental and thermodynamic results, are much more limited at deeper, subarc conditions (Connolly, 2005, Poli et al., 2009). Nevertheless, the role of fluid–rock interactions appears to be critical for the stability of carbonates. Recently, field based studies (Ague and Nicolescu, 2014; Frezzotti et al., 2011) as well as theoretical and experimental works (Facq et al., 2014, Sverjensky et al., 2014) have pointed out that massive carbonate dissolution in fluids may occur at high-pressure-low temperature conditions and can generate large amounts of carbonic fluids (see Kelemen and Manning, 2015 for review). Accounting for carbonate dissolution at high-pressure conditions in comprehensive budgets overturns older paradigms on carbonate stability with respect to carbon mobility in subduction zones. The most recent budgets actually predict that carbonate dissolution allows almost all subducted carbon to be transferred to the mantle wedge (Kelemen and Manning, 2015). Owing to the very recent discovery of these processes, much remains to be learned about the fate of these carbonic fluids and their interaction with slab- and mantle-forming rocks.

Here, we report the occurrence of eclogite-facies marbles formed by fluid–rock interaction processes (metasomatism) occurring along intensely metasomatized lithological interfaces (Alpine Corsica, France). We present and discuss the occurrence, textures, mineralogy and geochemistry of these metasomatic marbles. We then propose a mechanism of carbonates formation by precipitation and mineral carbonation by carbonic fluid–rock interactions at high-pressure conditions. Finally, the implications and contribution of rock carbonation to the deep carbon fluxes and cycling are discussed.

2. Geological setting

Alpine Corsica (France) is a branch of the Alpine orogenic system (Jolivet et al., 1991, Molli and Malavieille, 2011) (Fig. 1a). The belt mainly includes remnants of subducted Mesozoic slow-spreading oceanic and passive margin lithosphere, which formed part of the Tethys Ocean basin. This rock package is classically referred to as the Schistes Lustrés Complex (Fig. 1b; Jolivet et al., 1990, Fournier et al., 1991, Malavieille et al., 1998, Vitale Brovarone et al., 2013). The exceptional preservation of prograde-to-peak mineral assemblages, including widespread lawsonite, makes the Schistes Lustrés of Alpine Corsica an excellent site for field investigations related to subduction. These units underwent various metamorphic overprints during the Alpine subduction ranging from subgreenschist-facies conditions of about 300 °C and 0.5 GPa to lawsonite blueschist and lawsonite eclogite-facies conditions which reached 500–550 °C and ∼2.3 GPa (e.g. Fournier et al., 1991; see Vitale Brovarone et al., 2013 for review).

Carbonate-bearing rocks are widespread in the Schistes Lustrés of Alpine Corsica. The most typical carbonate-bearing lithologies are metamorphosed oceanic sediments (referred to as calcschists hereafter), ophicarbonate, and carbonated metabasalts (Miller et al., 2001, Ravna et al., 2010, Vitale Brovarone et al., 2011b). In each lithology, primary carbonates and various generations of carbonate veins are observed (Miller et al., 2001, Ravna et al., 2010, Vitale Brovarone et al., 2011a). These veins have been shown to be in most cases in isotopic equilibrium with the host rocks with little effect of external fluid infiltrations and metasomatism (Cartwright and Buick, 2000). On the other hand, evidence for high-pressure-low temperature fluid–rock interactions and metasomatism in the Schistes Lustrés of Alpine Corsica is widespread, most typically localized at lithological interfaces. In this work, we focus on processes occurring where serpentinites are in contact with metasedimentary rocks.

Here, past results on high-pressure metasomatism in Alpine Corsica are briefly summarized. In the blueschist-facies zone, reactions between serpentinites and overlying metasediments led to carbonate reduction and precipitation of wollastonite and abiotic graphite at blueschist-facies conditions (Malvoisin et al., 2012, Galvez et al., 2013a). Except for the influx of external, serpentinite-derived fluids, the reacted metasediments revealed largely conservative carbon budget (Galvez et al., 2013a). In similar lithological settings, massive precipitation of lawsonite from fluid–rock interactions at the expense of metasedimentary rocks in contact with serpentinites testifies to the reincorporation of large amounts of water in the rock at prograde

blueschist-to-eclogite-facies metamorphic conditions (Martin et al., 2011, Vitale Brovarone et al., 2014, Vitale Brovarone and Beyssac, 2014). This process is characterized by a dramatic whole-rock chemical modification leading to mafic/ultramafic, Ca-rich metasomatic products.

The carbonate-rich rocks studied herein are intimately related to the latter Ca-rich metasomatic rocks and were collected in the lawsonite eclogite-facies San Petrone unit. This unit is characterized by a basal body of serpentinite variably overlain by Jurassic pillow metabasalts, Mesozoic metasediments (e.g. calcschists, marbles, Mn-metacherts) or slivers of Hercynian continental basement rocks mainly consisting of pre-Alpine, carbonate-free, high-temperature metasediments and granitic rocks overprinted at high-pressure-low temperature conditions during the Alpine subduction (Vitale Brovarone et al., 2011b; Fig. 1c). Ophicarbonate rocks are locally found at the top of the serpentinite body. The San Petrone unit has been considered as a remnant of a Mesozoic hyper-extended passive margin (Vitale Brovarone et al., 2011b, Beltrando et al., 2014). Peak metamorphic conditions in this unit are estimated at ca. 490–530 °C and ∼2.3 GPa by means of pseudosection modeling and thermometry based on Raman spectroscopy of carbonaceous material (Ravna et al., 2010; Vitale Brovarone et al., 2011a, Vitale Brovarone et al., 2013). The peak metamorphic age of ∼34 Ma has been determined by several techniques including U–Pb zircon and Lu–Hf garnet and lawsonite geochronology (Martin et al., 2011, Vitale Brovarone and Herwartz, 2013).

3. Structural occurrence of metasomatic marbles

The carbonate-rich rocks which are the subject of this paper occur along a regional lithological boundary separating serpentinites from either slivers of Hercynian basement rocks (dominantly pre-Alpine high temperature metasedimentary rocks) or Mesozoic metasedimentary rocks (Figs. 1c and 2). The first few meters of rock above the serpentinites exhibit intense Alpine metasomatism that has already been described in previous studies (Martin et al., 2011; Vitale Brovarone et al., 2011b, Vitale Brovarone et al., 2014). These metasomatic rinds can be followed for several kilometers along the top of the serpentinite body and are characterized by lawsonite-rich assemblages, but diopside-rich rocks are also common. These rocks are referred to as Stage#1 diopside-lawsonite rocks (Fig. 2). The carbonated rocks which are the subject of this study are referred to as Stage#2 metasomatic marbles (or simply metasomatic marbles), these form discontinuous patches or lenses of variable thickness and lateral extension (from a few tens of cm to several m, Fig. 2), and are preferentially associated with diopside-rich rather than the lawsonite-rich metasomatic rocks. The petrological differences between Stage#2 metasomatic marbles and Mesozoic metasediments are discussed in Section 5.

The metasomatic marbles show a range of structural relationships with the surrounding diopside-lawsonite rocks, and the carbonate/host rock ratios are extremely variable. Fig. 2 summarizes the field relationships between the different rock types, i.e. serpentinites, Stage#1 diopside-lawsonite rocks, Stage#2 metasomatic marbles, and the inferred protolith rocks (continental basement rocks or Mesozoic metasediments). The transition from diopside-lawsonite rocks to Stage#2 metasomatic marbles is marked by a gradual increase of carbonate/host rock ratio, passing from diopside-lawsonite rocks to isolated carbonate-rich veins in Stage#1 host rocks, to Stage#2 metasomatic marbles with remnants of Stage#1 rocks. Isolated veins have crack-seal texture and are mainly composed of rod-shaped Ca-carbonate ± omphacite (Figs. 3a, b, d). Carbonate rods are perpendicular to the vein walls (Fig. 3b). Omphacite grows from the vein wall toward the center (Fig. 3d). Some veins exhibit interaction with the host Stage#1 rocks characterized by omphacite replacement of the precursor diopside (Al–Na gain; Ca–Mg loss) and local carbonate precipitation (Fig. 3d). The abundance of omphacite decreases from the vein wall to the host rock. Diopside far from the vein does not display any chemical zoning involving Na–Al enrichment. The isolated veins are connected to dm-thick layers (ca. 20 cm) showing similar crack-seal textures (Fig. 2, Fig. 3a). These layers are meter-scale and are parallel to the wallrock foliation (Fig. 2). Outcrop-scale hydraulic breccias consisting of cm- to m-scale angular clasts of Stage#1 diopside-lawsonite rocks embedded within a carbonate vein network provide strong evidence for diffuse hydrofracturing and carbonate precipitation (Fig. 2, Fig. 3e and f).

In some outcrops, serpentinites are overlain by a sequence of metasomatic marbles ranging in thickness from less than one m to ~10 m (Figs. 2, 3g and 4a). These metasomatic marbles are hosted within the diopside-lawsonite rock and contain remnants of the host rock—ranging from a few microns to several centimeters—floating in a carbonate-dominated matrix. Remnants of diopside-lawsonite rocks in the metasomatic marbles differ from the angular clasts found in the hydraulic breccias. First, they have embayed margins and microtextures (see Section 5) suggest digestion of the silicate portions into the carbonate matrix. Second, the host rock remnants preserve their original orientation (Fig. 4a), whereas the clasts in the hydraulic breccias have random rotation (Fig. 2). Last, the diopside remnants are commonly rimmed by omphacite, the latter being in textural equilibrium with the carbonate as observed in the isolated carbonate veins.

4. Methods

4.1. Scanning electron microscopy and electron microprobe

Petrographic thin sections were carbon coated for scanning electron microscopy (SEM). Observations were performed at a working distance of 7.5 mm using a Zeiss Ultra 55 field emission gun SEM operated at 15 kV with a 120 µm aperture. Backscattered electron (BSE) mode was used to investigate chemical heterogeneities using an Angle Selective Backscattered Detector (AsB) or an Energy Selective Backscattered Detector (EsB). Energy dispersive X-ray spectrometry (EDXS) maps were acquired using an EDXS QUANTAX system equipped with a silicon drift detector XFlash 4010 (Bruker). Data were processed with the software Esprit (Bruker). Mineral analyses were performed on a Cameca electron microprobe (either SX-100 or SX Five) (Camparis, Université Paris 6). Common analytical conditions were adopted for spot analyses [15 kV, 10 nA, wavelength-dispersive spectroscopy (WDS) mode], using Fe2O3, MnTiO3 (Mn, Ti), diopside (Mg, Si), orthoclase (Al, K), anorthite (Ca) and albite (Na) as standards. The automated Cameca ZAF procedure was used for quantification (Tables S1, S2, S4 and S5).

4.2. Whole rock major and trace element data

Chips of low to highly carbonated rock were removed from hand-samples. Samples were crushed in an agate mortar (grain size <80 µm) and sent for major and trace element, CO2 and organic carbon analyses at the Service d'Analyse des Roches et Minéraux (SARM, Centre de Recherches Pétrographiques et Géochimiques, Nancy, France) by alkali fusion of rock samples (LiBO2), followed by concentration measurements using an ICP-OES Icap 6500 (Thermoscientific) for major elements, and an ICP-MS X7 (Thermoscientific) for minor elements (protocol by Carignan et al., 2001). The modal proportions of silicates vs. carbonate were estimated first with optical microscopy and then checked using whole rock and mineral composition. In two cases, samples 1COR12-20d and COR13-29c, two different chips were taken: one representative of the metasomatic marble, where silicates are present as clasts, and another one representative of a Stage#1 diopside-lawsonite rock, where carbonate is a minor constituent. When an average value is indicated, the standard deviation (1σ) is also reported (Tables 1 and S2).

4.3. Carbon mass balance calculation

In/out carbon fluxes in the subducting slab (during high-pressure metamorphism) are estimated from the grams of CO2 per 100 g of rock released by decarbonation reaction and carbonate dissolution vs. the grams of CO2 per 100 g of rock bound by rock carbonation process (Section 8.3). The CO2 bound in the rocks of this study was back calculated from whole rock analyses removing the measured organic carbon content to the measured CO2 (red bar in Fig. 8a, see also Table S2). Values for CO2 released per 100 g of rock after carbonate dissolution (Ague and Nicolescu, 2014) and decarbonation of calcschists (Cook-Kollars et al., 2014) are taken from the literature. For the data on carbonate dissolution (Ague and Nicolescu, 2014), we took the average of the estimated CO2 loss in samples from Syros (35.1 g) and Tinos (22.2 g), thus resulting in 28.65 g of CO2 lost during carbonate dissolution (blue bar in Fig. 8a). For samples affected by decarbonation, we took the calcschist modeled by Cook-Kollars et al. (2014). This rock initially contains 40 wt.% carbonate (i.e. the initial

CO2 content is 17.6 g per 100 of rock) and it loses 50% of its initial CO2, thus 8.8 g per 100 g of rock (green bar in Fig. 8a). Cook-Kollars et al. (2014) highlighted that natural samples from Schist Lustrés and Cignana suite show a lower extent of decarbonation. They conclude that decarbonation reactions during metamorphism may cause the loss of 10 to 20% of the initial CO2. We took the intermediate value of 15%. Thus, considering the same initial CO2 content of 17.6 g per 100 g of precursor rock, the CO2 lost is 2.64 g per 100 g of rock (orange bar in Fig. 8a).

4.4. Stable isotope data

4.4.1. Carbon and oxygen isotope of calcite

Chips of carbonate were taken from hand-samples and crushed in an agate mortar. Raman and SEM analyses establish that the carbonate is nearly pure Ca-carbonate. The isotopic composition of calcite was measured by an AP2003 continuous flow mass spectrometer at LGIS, IPGP. Approximately 2 to 2.5 mg of sample were loaded in vials; three standards of pure calcite were also used for calibration of both concentration and isotopic composition. After flushing with ultrapure helium, orthophosphoric acid (H3PO4) was introduced in each tube in order to produce gaseous CO2. After 4 h of reaction at ambient temperature, calcite completely decomposes to release CO2 (McCrea, 1950); gases were then transferred into the mass spectrometer for analysis. In order to improve the precision of the measurements, each analysis was repeated four times for each vial, and each sample analyzed twice. The isotopic 13C/12C and 18O/16O ratios are expressed using the conventional δ-notation relative to PDB and SMOW international standards. The precision is 0.1‰ for $\delta^{13}C$ and 0.2‰ for $\delta^{18}O$. The results are reported in Table S3. When an average value is indicated, the standard deviation (1σ) is also reported.

4.4.2. Oxygen isotope of clinopyroxene

A polished sample of omphacite + carbonate vein hosted in diopside-lawsonite rock was first studied by SEM to identify zones representative of Stage#1 diopside and Stage#2 omphacite (Figs. 3d and S2). Aliquots of carbonate + omphacite vein were crushed (<100 µm) and single crystals of omphacite were separated by handpicking under a binocular microscope. Diopside-rich protolith rock was sampled out of the vein selvage (ca. 2 cm from the vein) in order to avoid the isotopic contribution of the vein-related omphacite rims, as checked by SEM. Rock was crushed (<100 µm) and single crystals of diopside were separated by handpicking under a binocular microscope. Approximately 2 mg of omphacite and 2 mg of diopside were analyzed using laser fluorination at IPGP (Paris, France) along with UWG-2 garnet standard. Analytical methods are similar to those documented in Rumble et al. (1997). The oxygen isotopic ratios are reported using the international V-SMOW standard. Measurement of UWG-2 garnet standard aliquots gave 2σ external error on $\delta^{18}O$ of 0.036‰ , which is in the same range of in-run uncertainties for individual measurements (<0.03‰). Measurements were duplicated for omphacite, while for diopside the material collected was not sufficient. Fractionation factors (Hoffbauer et al., 1994) were used to infer oxygen isotope equilibrium temperature between carbonate and clinopyroxenes (Table S3.1). Estimated errors using a Monte Carlo simulation on the calculated temperatures are 30 °C and 20 °C for the omphacite-calcite and diopside-calcite equilibrium, respectively.

5. Petrography of selected metasomatic marbles

Metasomatic marbles have characteristic features that make them different from any other carbonate-bearing rocks of the Schistes Lustrés (i.e. Mesozoic impure marbles, calcschists and ophicarbonates), although they may display mineralogical and chemical variations from one to another outcrop. As an example, the matrix carbonate in these rocks systematically displays a rod-shaped habit with rods oriented at high angles to the regional schistosity or to the margin of Stage#1 clasts in hydraulic breccias (Fig. 3b). In all but one metasomatic marble, the carbonate is a Ca-carbonate phase. Matrix carbonate is calcite, whereas aragonite was found as inclusions in garnet and apatite (see Fig. S1). Dolomite was detected in only one

sample by Raman spectroscopy and it was in very small proportions compared to Ca-carbonate (dolomite content below X-ray diffraction detection limit). No ankerite was observed in these rocks, whereas it is common in calcschists and ophicarbonates of the Schistes Lustrés. As Ca-carbonate is the dominant carbonate phase, we will use hereafter the term "carbonate" to indicate compositionally pure Ca-carbonate (i.e. calcite after aragonite).

In thin section, metasomatic marbles display a characteristic structure defined by carbonate-rich and diopside-lawsonite-rich domains, the latter occurring as either continuous layers or isolated patches (Figs. 4b, d, e). A compositional layering is defined by the alternation of carbonate aggregates with diopside (±lawsonite) aggregates. Calcite rods are mm-sized; diopside and lawsonite grain size ranges from µm to mm. The mineral assemblage most commonly consists of carbonate, diopside and lawsonite, with modal proportions varying from sample to sample (Fig. 4). Garnet is also present in several samples. It is found as euhedral, µm to mm-sized crystals in textural equilibrium with carbonate. Its composition ranges from grossular to almandine-spessartine solid solution (Table S4). Phengite, epidote, quartz and pumpellyite (Table S5) are also present. Common accessory phases are titanite, apatite and graphite. Although such assemblages are described in calcschists in the Western Alps (see e.g. Cook-Kollars et al., 2014), they have never been documented in Alpine Corsica to our knowledge. Moreover, the textural and mineralogical features of these silicates indicate that they resulted from intense metasomatism during their high-pressure evolution, as described below.

For simplicity, two dominant mineralogical assemblages representative of Stage#1 and Stage#2 rocks are distinguished, i.e. diopside + lawsonite and carbonate + omphacite, respectively. As mentioned above, additional phases may be present from one sample to another. The chronological relations between the two mineralogical assemblages may be deciphered from the outcrop-scale down to the micro-scale. Diopside (Quadrilateral96.5 Aegirine3.5; classification after Morimoto, 1988; see Tab. S1) formation at high-pressure conditions during subduction is demonstrated by: (i) the occurrence of diopside veins cross-cutting lawsonite-bearing fabrics (Fig. 3d) and (ii) the fact that the diopside veins are in turn cut by carbonate + omphacite veins, indicating near peak P–T metamorphic conditions. In the carbonate-bearing domains, diopside in contact with carbonate shows either embayed grain boundaries or newly-formed compositional coronas of omphacite (Fig. 5a; Jadeite39.5 Quadrilateral44.5 Aegirine16; see Table S1). Tiny (ca. 10–20 µm), second generation idioblastic lawsonite crystals were locally found in the carbonate. In the vein selvage, omphacite rims on diopside (Fig. 5b) have the same composition as omphacite growing together with carbonate in the vein. In metasomatic marbles, atoll-like textures show relict diopside cores being replaced by carbonate and rimmed by omphacite (Fig. 5a), the latter being in textural equilibrium with the carbonate matrix. The abundance of omphacite varies from one sample to another. All transitional stages from carbonate-free diopside-lawsonite rocks to carbonate-rich rocks are depicted in Fig. 4.

Only one sample (COR13-21d) displays a different mineralogy, composed of (in order of volume abundance): calcite, actinolite, chlorite and clinopyroxene. This sample was collected within a sequence of typical metasomatic marbles, and shares with them similar characteristic features such as rod-shaped carbonate and Na-rich clinopyroxene coronas (aegirine-augite, Na–Fe3+ rich clinopyroxene, see Fig. 5c) on relict diopside. Geochemical data for this sample are given in Section 6.

6. Whole rock chemical composition

Samples of metasomatic marbles were analyzed for their major and trace element bulk composition (Table S2). Reference samples of Mesozoic calcschist and ophicarbonate unaffected by metasomatism (i.e. far from the studied lithological boundaries and showing no mineralogical or textural evidence for fluid–rock interactions), were also analyzed (Table S2). Table 1 reports the average major element composition of metasomatic marble as well as the compositions of a Stage#1 diopside-lawsonite rock (sample OF3598 in

Vitale Brovarone et al., 2014) and a Stage#1 rock with higher lawsonite content (lawsonite mode ca. 75%; sample COE5, Martin et al., 2011).

The variability of both Stage#1 rocks and Stage#2 metasomatic marbles hampers quantitative mass balance calculation. Here, only concentrations of the most representative oxides CaO, MgO, SiO2 and CO2 are presented. Metasomatic marbles have variable compositions based on the carbonate-silicate modal proportions (Tables 1, S2). The average composition is: CaO 39 wt.% (±5%, 1σ); CO2 27 wt.% (±6%, 1σ); SiO2 20 wt.% (±6%, 1σ) and MgO 3 wt.% (±2%, 1σ). The silicate mode in sample COR13-21d is higher, thus resulting in a slightly different bulk rock composition (CaO 22%; CO2 12%; SiO2 37%). Even accounting for the lower carbonate content, sample Cor13-21d has an Mg-richer composition (MgO 11 wt.%) compared to metasomatic marbles.

Comparing the average composition of metasomatic marbles with Stage#1 diopside-lawsonite rock (Table 1), the following features can be outlined. Despite the variability of the protolith (with more or less abundant lawsonite), CaO is always enriched (CaO in metasomatic marbles is about double that in Stage#1 rocks). MgO variations are more difficult to evaluate, as they depend not only on the silicate content of metasomatic marbles, but also on the initial diopside modal proportion of Stage#1 rock (cf. samples OF3598 and COE5, Table 1). The reference calcschist (sample COR13-32) fits the range of compositions of Alpine calcschists (Busigny et al., 2003, Galvez et al., 2013b). The reference ophicarbonate sample (sample COR13-30a), has a Mg-rich composition (13 wt.% vs. 3 wt.% in metasomatic marbles), similar to sample COR13-21d.

Whole-rock Rare-Earth Element (REE) analyses of most analyzed samples have positive slopes (LaN/LuN > 1) comparable to the reference calcschist and the host diopside-lawsonite rock formed at the expense of carbonate free, continental basement metasedimentary rocks (Fig. 6; Martin et al., 2011, Vitale Brovarone et al., 2014). Only sample COR13-21d differs significantly. It has a rather flat REE pattern, except for a slight negative Ce anomaly (Fig. 6). This pattern matches reasonably well with the ophicarbonate standard and passive margin serpentinites (Barnes et al., 2014, Deschamps et al., 2013; Kodolányi et al., 2012). This sample also has a significantly higher Ni and Cr content than the other analyzed samples (1022 and 2114 ppm respectively, Table S2). These patterns suggest an ultramafic signature for this sample.

7. Carbon and oxygen stable isotope analysis of Ca-carbonate and clinopyroxene

C and O isotopic compositions of calcite from metasomatic marbles (including veins) were analyzes, as well as the O isotopic compositions of Stage#1 diopside and Stage#2 omphacite. For reference, calcite from calcschist and ophicarbonate was also analyzed. Analyses of carbon and oxygen isotope of calcite are reported in Table S3.

For all samples (reference calcschists and ophicarbonate as well as metasomatic marbles) calcite $\delta^{13}C$ values vary little and average 1.1‰ (±1.2, 1σ) (Fig. 7a), consistent with marine sedimentary carbonate rocks (Plank and Langmuir, 1998). The average calcite $\delta^{18}O$ value of metasomatic marbles is 14.3‰ (±3.2, 1σ) (Fig. 7a). The two reference calcschists (from ca. 8 to 50 m from the serpentinite, across strike) have an average $\delta^{18}O$ of 21.5‰ (±1.5, 1σ). The ophicarbonate analyzed in this study has $\delta^{18}O$ of 11‰. Carbonate in veins cutting across carbonate-free, diopside-rich rocks has very low $\delta^{18}O$ 10.6‰ (±0.2, 1σ), independent of vein distance from the serpentinite. Carbonate in samples collected from outcrops with higher carbonate/silicate ratios (e.g. carbonate mode 70%) display more dispersed values that vary from ~12 to ~18‰. In these rocks, samples collected a few centimeters from the serpentinite body have an average value of ~14‰ (9 samples), whereas the two samples collected far from the serpentinite (i.e. more than 3 m) and within the analyzed interaction zone (cf. Figs. 6 and S3 and Table S3 for sample location and respective REE patterns and isotope composition) have a heavier signature of ~18‰. A simple correlation cannot be established between the distance from the serpentinite and the $\delta^{18}O$ values within the reaction zone. Indeed, Stage#2 omphacite-carbonate veins far from the serpentinite body (up to 8 m from the contact) have low $\delta^{18}O$ values similar to metasomatic marble sampled a few cm from the serpentinite body (e.g. samples 2COR14-4i and 1COR14-

11a; Table S3). However, taken as a whole, metasomatic marbles, overlying the serpentinite body, have lower $\delta^{18}O$ compared to the reference calcschists. Indeed, calcschists that lack the petrographic characteristics of intense fluid–rock interaction present in metasomatic marbles always have heavier values (ca. 21‰, see samples COR13-32 and 1COR12-11Q, Table S3), even if they crop out at less than 1 m from the metasomatic zones.

Reconnaissance oxygen isotope measurements on silicate minerals were performed in order to test for isotopic equilibrium between the two clinopyroxene generations (Stage#1 diopside and Stage#2 omphacite) and the vein infill carbonate. The analyzed sample is composed of the host Stage#1 diopside-rich rock cut across by a Stage#2 calcite-omphacite vein (Figs. 3d and S2). Diopside has $\delta^{18}O$ values of ~6‰. Vein infill omphacite has heavier $\delta^{18}O$ of ~7‰. Fractionation factors available from literature data ($\Delta^{18}O$calcite-clinopyroxene from Hoffbauer et al., 1994, Table S3.1), give equilibrium temperature of 494 °C (±30 °) for the omphacite-carbonate assemblage and 426 °C (±20°) for diopside-carbonate using the same database. These differing temperatures are consistent with textural disequilibrium between the mineral pairs (carbonate-diopside and diopside-omphacite). The omphacite-calcite thermometer yields temperatures closer to the estimated peak T conditions of the metamorphic unit (490–530 °C, see Section 2). This observation suggests isotopic equilibrium for the omphacite + carbonate paragenesis and confirms the microtextural observations (see Section 5).

Equilibrium was likely reached by fluid-mediated reactions. However, this interpretation must be taken with caution because only one sample was analyzed. The composition of an aqueous fluid in equilibrium with these minerals was also calculated at 500 °C (i.e. near peak conditions). The $\delta^{18}O$ of a fluid in equilibrium with the measured Ca-carbonate is 10.1‰ ($\Delta^{18}O_{cal\ -H2O}$= 0.62, Zheng, 1994). For the analyzed omphacite composition, the water $\delta^{18}O$ obtained is 8.4‰ ($\Delta^{18}O_{di\ -H2O}$ =-1.95, $\Delta^{18}O_{ae\ -H2O}$ =-0.07 and $\Delta^{18}O_{jd\ -H2O}$ =- 0.14, Zheng, 1993). Although the fractionation factors for lawsonite are not available, the diopside-water equilibrium, can be used as a proxy for fluid in equilibrium with the Stage#1 assemblage implying that the fluid $\delta^{18}O$ = 8‰. The mismatch between calcite-water and omphacite-water oxygen composition equilibrium is quite small as well as for water in equilibrium with diopside. It is worth noting that the estimated fluid composition is similar for both metasomatic stages.

8. Discussion

8.1. Fluid-mediated carbonation at high-pressure conditions

Detecting metasomatism in metasedimentary rocks is often challenging owing to the variability of protolith compositions (Bebout and Barton, 1989, Ague, 2003). The occurrence of carbonate in metasedimentary rock is common, and in most cases likely reflects the primary composition of the subducted rocks. However, the direct spatial association of Stage#2 metasomatic marbles along major fluid conduits characterized by intense metasomatism (Martin et al., 2011, Vitale Brovarone et al., 2014) suggests that the evolution of these rocks was mediated by the interaction with external fluids (e.g. Ague, 2003).

Rod-shaped calcite crystals in marbles from eclogite-facies terrains have been described in Syros (Greece) and the Sivrihisar belt (Turkey) (Brady et al., 2004, Seaton et al., 2009), and have been interpreted as topotactic pseudomorphs of calcite after aragonite. Both studies regard carbonate as a primary constituent of the rock and do not consider fluid-mediated precipitation. In the study case, we consider this hypothesis unlikely based on several lines of evidence. Textures like crack-seal and networked carbonate veins cutting across carbonate-free metasomatic rocks suggest high pore fluid pressure and hydrofracturing (e.g. Bebout and Barton, 1989). This evidence clearly points to the percolation of carbonic fluids along lithological boundaries, and their precipitation of carbonate. As reported in Sections 2 and 5, field relations and microstructural features (Figs. 4) suggest carbonation of the Ca–Mg-rich silicate rocks. The lateral (along schistosity) transition from carbonate-free diopside-lawsonite rocks and metasomatic marbles is evidence for chemical interaction occurring between a carbonic fluid and the host-rock assemblage. Progressive

replacement of diopside-rich rocks by carbonate is demonstrated at the microscale by the corroded texture of precursor minerals (embayed and atoll-like diopside, Figs. 4d, e and 5a) and producing coronas in contact with carbonates (e.g. omphacite rims on diopside, Figs. 5a and b). The carbonate isotopic composition presented in this work (Section 7) further supports the hypothesis of fluid-mediated carbonate precipitation. All metasomatic marbles are composed of Ca-carbonate (calcite after aragonite). This appears unlikely in the case of metamorphic recrystallization of rocks containing significant whole rock Mg (Table S2). These observations suggest that carbonate precipitation occurred via two concurrent processes of fluid–rock interaction: crack-sealing (carbonation by volume increase, Section 3) and mineral replacement (Section 5). Note that carbonation of mafic rocks during high-pressure metamorphism was also suggested by Boundy et al. (2002) for eclogite-facies rocks from the Lindås Nappe (Caledonides, Western Norway) and by Kleine et al. (2014) for blueschist-facies rocks from Syros. Both authors proposed carbonation of mafic eclogites along a shear zone affected by fluid circulation. Similarly, Nishiyama (1990) proposed metamorphic carbonation during exhumation of blueschist-facies metabasic rocks in association with serpentinites in the Nishisonogi metamorphic complex (Japan).

Based on these observations, the metasomatic history of the Corsican eclogite-facies marbles can be subdivided into two stages, both occurring at high-pressure conditions during subduction.

Stage#1: calcic metasomatism of protolith metasedimentary rocks or continental basement transforms metasediments in contact with serpentinites to Ca–Mg rocks dominantly composed of diopside and lawsonite during prograde metamorphism (cf. Martin et al., 2011, Vitale Brovarone et al., 2014).

Stage#2: carbon-bearing fluid reacts with the pre-existing diopside-lawsonite rock and associated serpentinites leading to the precipitation of carbonate-dominated assemblages as either crack-filling material, or by replacing silicate minerals. The metamorphic conditions for this stage are constrained to high-pressure conditions by the assemblage aragonite + omphacite + lawsonite + garnet that characterize several of the analyzed samples (P > 1.5 GPa at 450–500 °C), and supported by the estimated O isotope Ca-carbonate-omphacite equilibrium T of ca. 500 °C.

8.2. Stable isotope: marker of rock carbonation and fluid source?

Stable isotope geochemistry has provided important information for the study of high-pressure metasomatic processes involving carbonates (Valley, 1986, Wang and Rumble, 1999, Ague and Nicolescu, 2014, Galvez et al., 2013a, Galvez et al., 2013b). The trends of decreasing $\delta^{13}C$ and $\delta^{18}O$ isotopic composition of the metamorphic carbonates may be attributed to: (i) inheritance of protolith isotopic signatures (Wang and Rumble, 1999), (ii) carbonate-silicate isotopic exchange; (iii) devolatilization reactions driven by increasing temperatures (Wang and Rumble, 1999), or (iv) interaction with COH fluids (Ague and Nicolescu, 2014, Galvez et al., 2013a, Galvez et al., 2013b).

In this study, hypothesis (i) can be ruled out by comparison of the isotopic signature of metasomatic marbles with calcschists far from the metasomatic zones. The reference calcschists have $\delta^{13}C$ values of ca. 0‰ and $\delta^{18}O$ of ca. 21‰ similar to those of calcschists and carbonate veins (for similar metamorphic conditions) in Alpine Corsica (Cartwright and Buick, 2000, Miller et al., 2001), Western Alps (Cartwright and Barnicoat, 1999, Cook-Kollars et al., 2014), and Cyclades (Ague and Nicolescu, 2014) (Fig. 7a). The metasomatic marble $\delta^{13}C$ values are shifted toward heavier values, although still overlapping the compositional range of seawater carbonates, whereas $\delta^{18}O$ values display a much greater dispersion towards lower values (Fig. 7a).

Partial silicate-carbonate oxygen isotope exchange (hypothesis ii) is an alternative way to explain low $\delta^{18}O$ (with almost no change in $\delta^{13}C$). We discard this scenario for two reasons. 1) At temperatures of 500 °C, isotopic exchange by diffusion between two solid phases is expected to be very slow and thus restricted to

grain margins. 2) Even if interface-coupled dissolution precipitation allowed faster isotopic exchange (Putnis and John, 2010), the $\delta^{18}O$ achieved in the carbonate after such equilibration should be correlated with the silicate content (the lowest $\delta^{18}O$ being observed for the highest silicate content; Wang and Rumble, 1999, Cook-Kollars et al., 2014). Fig. 7b shows that no correlation exists between the $\delta^{18}O$ of carbonate and the silicate content in the rock.

As a test for the third hypothesis, the metasomatic marbles are compared with carbonates that have experienced devolatilization reactions. Carbonates in skarns formed by contact metamorphism are characterized by a strong decrease of $\delta^{13}C$ coupled with a smaller $\delta^{18}O$ decrease during decarbonation (e.g. Valley, 1986). The trend observed in Corsican metasomatic marbles of $\delta^{18}O$ decreasing with $\delta^{13}C$ remaining constant is actually different from a devolatilization trend (Fig. 7c).

Considering the compelling evidences for fluid–rock interactions and metasomatism, interactions between rocks and COH fluids (hypothesis iv) is considered the most likely hypothesis. Galvez et al. (2013b) reported carbonate reduction to graphite in contact with serpentinites in the high-pressure units of Alpine Corsica. In this study, carbonates display a peculiar variation showing a decreasing $\delta^{18}O$ coupled with increasing $\delta^{13}C$. Residual carbonate in samples affected by carbonate dissolution driven by serpentinite-derived fluids described by Ague and Nicolescu (2014) show a drop in oxygen isotopic signature compared to the protolith (6 to 10‰ lower values). However, changes in $\delta^{13}C$ are very small, with only a 1.5‰ decrease. Both carbonate precipitation and dissolution seem to be characterized by a large decrease in $\delta^{18}O$ and little to no change in $\delta^{13}C$ (Fig. 7c; cf. Section 8.3 for additional discussion). The $\delta^{13}C$ values of metasomatic marbles are similar to those typical of carbonates in marine sediments (e.g. Hoefs, 2013) and subducted oceanic suites ($\delta^{13}C$ close to 0‰; e.g. Miller et al., 2001), thus indicating that carbon in the fluids derives from marine carbonates, likely from the overlying carbonate-bearing metasedimentary rocks. The low $\delta^{18}O$ values rather point to fluids equilibrated with silicates in mafic or ultramafic rocks, possibly including Stage#1 metasomatic rocks (Miller et al., 2001, Martin et al., 2014, Vitale Brovarone et al., 2014, Angiboust et al., 2014). The large serpentinite body in contact with the rocks of this study would represent a plausible source for aqueous fluid with a light oxygen signature. Despite the lack of evidence for serpentinite dehydration (e.g. metamorphic olivine) in the samples from Alpine Corsica, a growing number of studies (Faccenda, 2014, Wilson et al., 2014) have proposed that fluids generated at depth can move up along the plate interface and interact with shallower slab-forming rocks. Ague and Nicolescu (2014) proposed that fluid equilibrated with mafic and ultramafic rocks can drive stoichiometric carbonate dissolution, resulting in aqueous fluid enriched in carbon with $\delta^{13}C$ around 0‰. However, if fluids were diluted, the contribution of oxygen from dissolved carbonates to the oxygen isotopic signature of the fluid is expected to be very low. The preservation of lawsonite requires very low X_{CO2} fluid concentrations ($X_{CO2} < 0.005$; e.g. Nitsch, 1972), demonstrating that the carbon-bearing fluid was dominantly aqueous. Altogether, these considerations point to metasomatic marbles formation by interaction with aqueous fluids bringing isotopic signatures of both dissolved carbonates and mafic/ultramafic reservoirs.

8.3. Rock carbonation during subduction: implications for the deep carbon cycle

The behavior of carbonate, more specifically Ca-carbonate, during subduction has long been a matter of debate. Few experimental studies of Ca-carbonate solubility in H_2O have been conducted at P–T conditions appropriate for subduction metamorphism (Walther and Long, 1986, Fein and Walther, 1989, Newton and Manning, 2002, Caciagli and Manning, 2003, Manning et al., 2013, Facq et al., 2014). Caciagli and Manning (2003) showed that calcite solubility increases with P and T at high-pressure conditions. Ca-carbonate dissolution at high-pressure conditions has been demonstrated to be very efficient in natural environments (P> ~ 2 GPa , Frezzotti et al., 2011, Ague and Nicolescu, 2014), and it is now considered as a major process for the mobilization of carbon in subduction zones (Kelemen and Manning, 2015). Carbonic fluids produced by carbonate dissolution are thus a potential source of carbon for carbonate precipitation in subduction zones. Fig. 8a shows a rough carbon fluxes mass balance (see Section 4.3 for method of carbon fluxes

calculation) considering carbon bound by rock carbonation in metasomatic marbles vs. the amount of carbon dioxide released by dissolution and devolatilization reactions estimated in previous field-based studies in analog geological settings (Ague and Nicolescu, 2014, Cook-Kollars et al., 2014). The amount of CO2 released by decarbonation (green and orange bars) is small compared to that released by dissolution (blue bar). Consequently, processes related to carbonate solubility mobilize carbon in greater quantities than simple decarbonation reactions (Ague and Nicolescu, 2014). A possible explanation for this result is that devolatilization reactions are controlled and limited by the presence of silicate phases with which the carbonate minerals can react, regardless of the fluid fluxes. The red bar in the diagram indicates the inferred amount of CO2 transferred from the fluid to the rock by rock carbonation, considering an initial carbon content of 0 g per 100 g of precursor rock. The amount of carbon bound per 100 g of rock is directly comparable with that released by carbonate dissolution. This observation suggests that a large amount of dissolved carbon can be re-bound into the solid phase by rock carbonation, and that carbonate dissolution and rock carbonation at high-pressure conditions are both crucial processes controlling carbon fluxes during subduction.

Slab-parallel ascent of fluids may represent a suitable configuration to enhance the efficiency of rock-carbonation reactions, if favorable conditions occur (Lazar et al., 2014, Kelemen and Manning, 2015, Sverjensky et al., 2014). Fig. 8b shows the Ca-carbonate solubility in aqueous fluid as a function of P and T (after Kelemen and Manning, 2015) along with the predicted P–T path for cold subduction (after Syracuse et al., 2010). Deep metamorphic fluids ascending parallel to the downgoing slab would cut across the solubility curves during their ascent. Although prediction of fluid slab-parallel ascent by numerical modeling is still limited (e.g. Faccenda, 2014, Wilson et al., 2014), natural samples from high-pressure (this study) and ultrahigh-pressure exhumed metamorphic terrains may preserve records of the interactions of deep-fluids with the slab-forming rocks. In this study, it is shown how major lithological interfaces (e.g. crust-metasediments) may represent ideal settings for fluid channelization. In addition, the data presented here also show that Ca–Mg-rich rocks (diopside-rich) and ultramafic rocks are reactive lithologies for rock carbonation at high-pressure conditions.

Interaction between slab-derived fluids and mantle-wedge rocks also represents a possible lithological configuration for rock carbonation. High amounts of carbonic fluids resulting from slab carbonate dissolution are expected to percolate through the mantle wedge, where ultramafic rocks may represent a suitable reactant (Kelemen and Manning, 2015). Based on the current knowledge of processes occurring along the plate interface (e.g. Syracuse et al., 2010), carbonation of the hydrated mantle wedge overlying subducting slabs seems unlikely in the case of vertical upward migration (rising T), whereas it is more plausible along the slab-mantle interface (decreasing T). Exhumation of cold serpentinite diapirs in forearc settings may also be a possible environment for rock carbonation (Fryer et al., 1992). Future studies on rocks ascribed to the mantle wedge are needed to test this hypothesis.

9. Conclusions

The petrological and geochemical results of this study indicate that the Corsican eclogite-facies marbles found along major fluid conduits have a metasomatic origin and were formed at high-pressure conditions during subduction. These rocks formed by carbonation of Ca–Mg silicate rocks by percolating carbonic fluids (Fig. 9). This implies that carbonic fluids formed during prograde carbonate dissolution may not be directly and fully transferred to the mantle wedge, but can also flow along slab interfaces (i.e. crust-metasediments) and reprecipitate carbonates under favorable conditions in both slab- and mantle-forming rocks. Carbonates precipitating from these fluids then display a characteristic geochemical and isotopic signature. Therefore, carbonation of Ca–Mg silicate rocks at high-pressure-low temperature conditions can be an efficient process to lock carbon in the rock, as is well documented at shallow and seafloor conditions (Guyot et al., 2011, Matter and Kelemen, 2009). The widespread occurrence of these rocks in the units of Alpine Corsica is likely a consequence of the overall exceptional preservation of pristine high-pressure-low temperature

assemblages in this belt. This suggests that analogous rocks and processes may have occurred in more retrogressed high-pressure belts, such as the Western Alps, the Cyclades and Turkey, and may be happening today in present-day subduction zones as well.

Whether or not high-pressure rock carbonation permanently binds carbon in the rock cannot be easily established at present. For example, high-pressure carbonated rocks can experience successive carbonate dissolution in deeper parts of subduction zones. Nonetheless, carbonation of slab- and mantle-forming rocks (Fig. 9) likely modulates the residence time of carbon in different reservoirs, and can modify the oxygen and carbon isotopic signature of carbonates in subduction zones. Considering a longer time-scale perspective (e.g. time elapsed from subduction initiation to continental collision), carbonation at high-pressure conditions may ultimately influence the fluctuation of CO2 emissions at volcanic arcs during the life of a subduction zone, and thereby the fluctuation of atmospheric CO2 over geological time scales (e.g. Berner and Kothavala, 2001).

Acknowledgments

The research leading to these results has received funding from the Deep Carbon Observatory, the University Pierre et Marie Curie (Paris 6) and Sorbonne Universités. Imène Esteve and Sébastien Charron are thanked for their technical support in the SEM platform. Benoit Baptiste is thanked for his technical support in the XRD platform. The purchase of the Scanning Electron Microscope (SEM) facility of the Institut de Minéralogie, de Physique des Matériaux et de Cosmochimie (IMPMC) was supported by Région Ile de France grant SESAME 2006 N∘I-07-593/R, INSU-CNRS, INP-CNRS, University Pierre et Marie Curie – Paris 6, and by the French National Research Agency (ANR) grant no. ANR-07-BLAN-0124-01. Michel Fialin and Nicolas Rividi (CAMPARIS service) are thanked for their technical support during electron microprobe measurement. Anonymous reviewers and the journal editor M. Bickle are thanked for their careful and constructive reviews on this manuscript.

Sample	**Metasomatic marble** (n=4)	**1σ**	**OF3598**[a]	**COE5**[b]
			Stage#1 rock	
SiO_2	20.44	5.65	45.30	40.6
Al_2O_3	4.97	2.94	15.11	25.6
Fe_2O_3	3.22	1.14	5.03	2.28
MnO	0.18	0.16	0.11	0.13
MgO	3.14	1.77	6.95	1.8
CaO	39.23	5.32	20.62	17.65
Na_2O	0.92	0.95	0.47	0.51
K_2O	0.12	0.16	0.01	0.24
TiO_2	0.18	0.11	0.65	1.94
P_2O_5	0.09	0.04	0.11	0.41
LOI	27.05	5.12	5.57	7.94
Tot	99.54		99.94	99.10

a From Vitale Brovarone et al. (2014).

b From Martin et al. (2011).

Table 1. Whole rock major element composition for metasomatic marbles (see Table S2 for details), Stage#1 diopside-lawsonite rock (OF3598) and Stage#1 rock with lawsonite >70% (COE5).

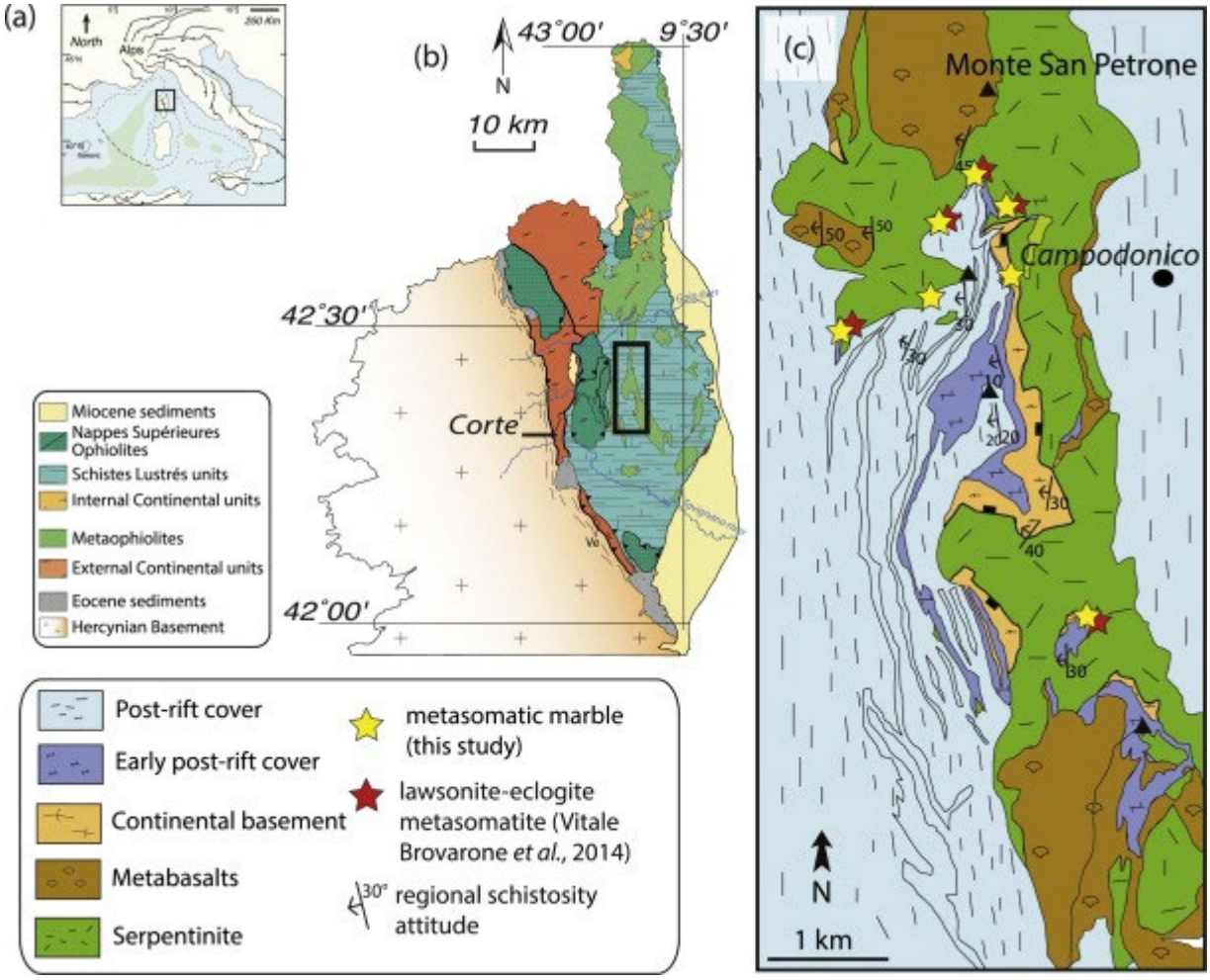

Fig. 1. Geological background of the study area. a) Simplified regional setting of Alpine Corsica (France) in the Western Mediterranean region. Modified after Molli and Malavieille (2011). b) Simplified tectono-stratigraphic map of Alpine Corsica. The black box indicates the position of the study area. c) Simplified geological map of the San Petrone unit. Figures modified after Vitale Brovarone et al., 2011b, Vitale Brovarone et al., 2013.

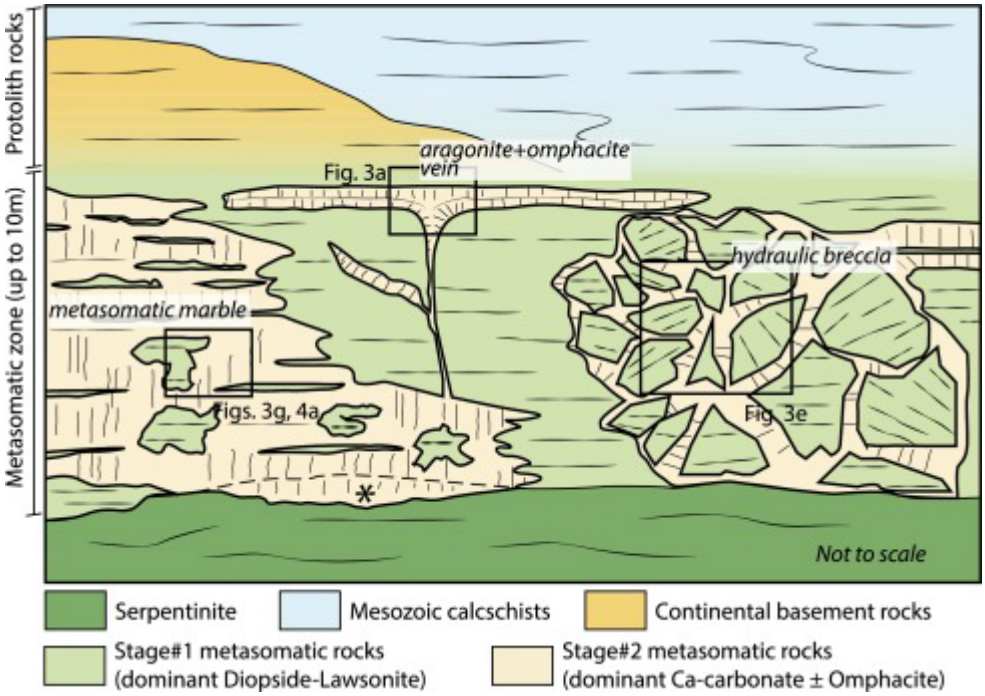

Fig. 2. Simplified structural sketch summarizing the field relationships between the different rock types and the location of the study samples. The star refers to metasomatic marbles formed at the expense of former serpentinites.

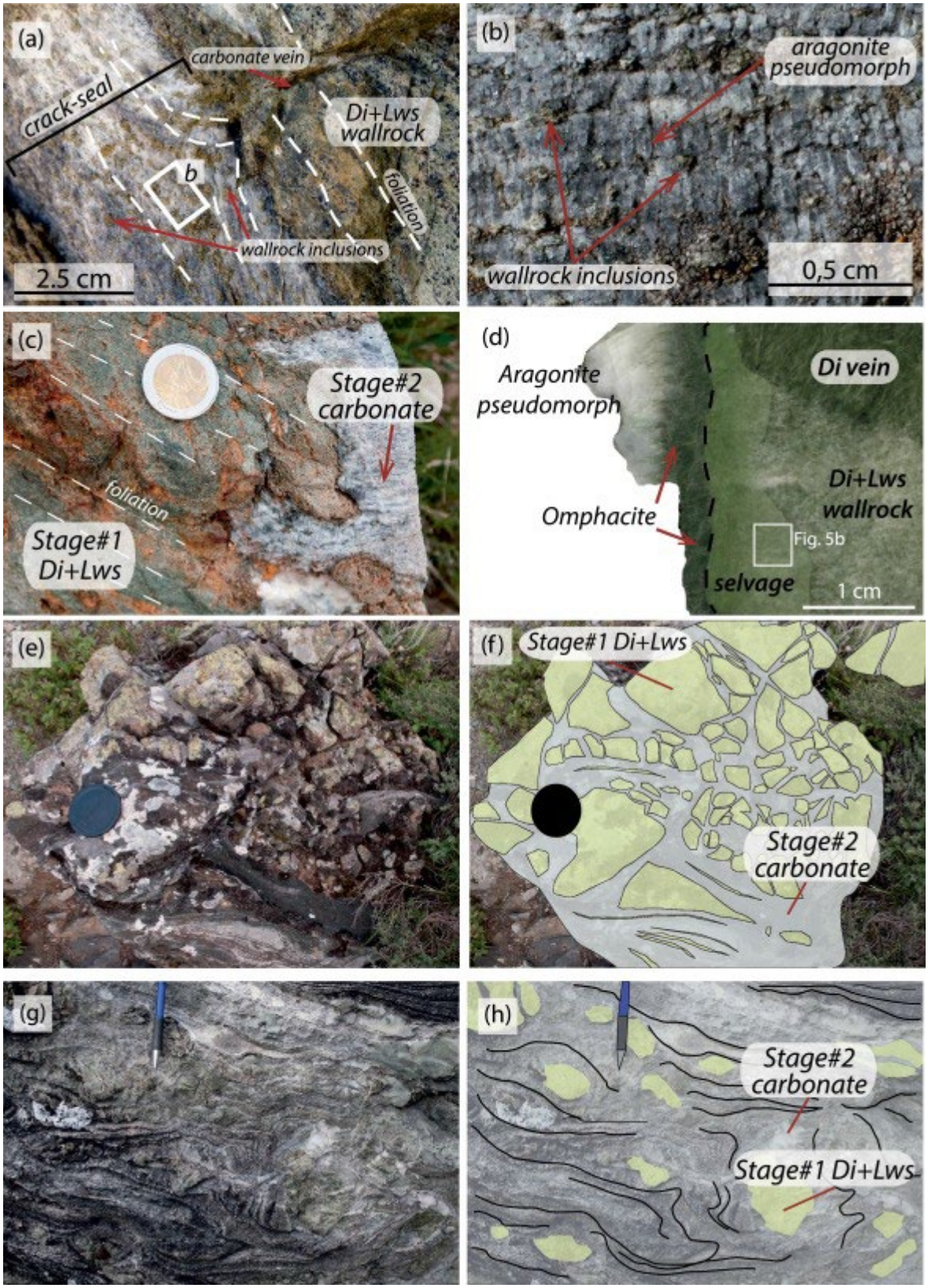

Fig. 3. Representative textural features of metasomatic marble in the field. a) Crack-seal texture in a metasomatic marble lens located in the metasomatic rind formed along the continental basement-serpentinite contact. Dashed lines mark the schistosity in the host rock and the orientation of the remains of the host rock in the carbonate-rich domain (see detail in b). Note that the silicate layers are deflected toward the carbonate vein. b) Detail of carbonate layers containing rod-shaped aragonite pseudomorphs alternating with vein-parallel bands of wallrock inclusions. c) Interdigitation of rod-shape carbonate with Stage#1

diopside-lawsonite rock. d) Carbonate + omphacite vein cutting across Stage#1 diopside-lawsonite rock. The black dotted line marks the vein wall and the green area overdrawn marks the selvage extension. e) and f) Photograph and related interpretative sketch of a hydraulic breccia (types defined by Jébrak, 1997) consisting of angular clasts of diopside-lawsonite rock (Stage#1 metasomatism) sealed by a network of veins containing rod-shaped carbonate crystals. g and h) Outcrop with high carbonate/silicate ratio and corresponding sketch. Rounded chunks of Stage#1 diopside-lawsonite rock float in a carbonate matrix. Microtextures in the carbonate-rich domains suggest digestion and chemical replacement of Stage#1 silicates by carbonate. Di = diopside; Lws = lawsonite. (For interpretation of the references to color in this figure legend, the reader is referred to the web version of this article.)

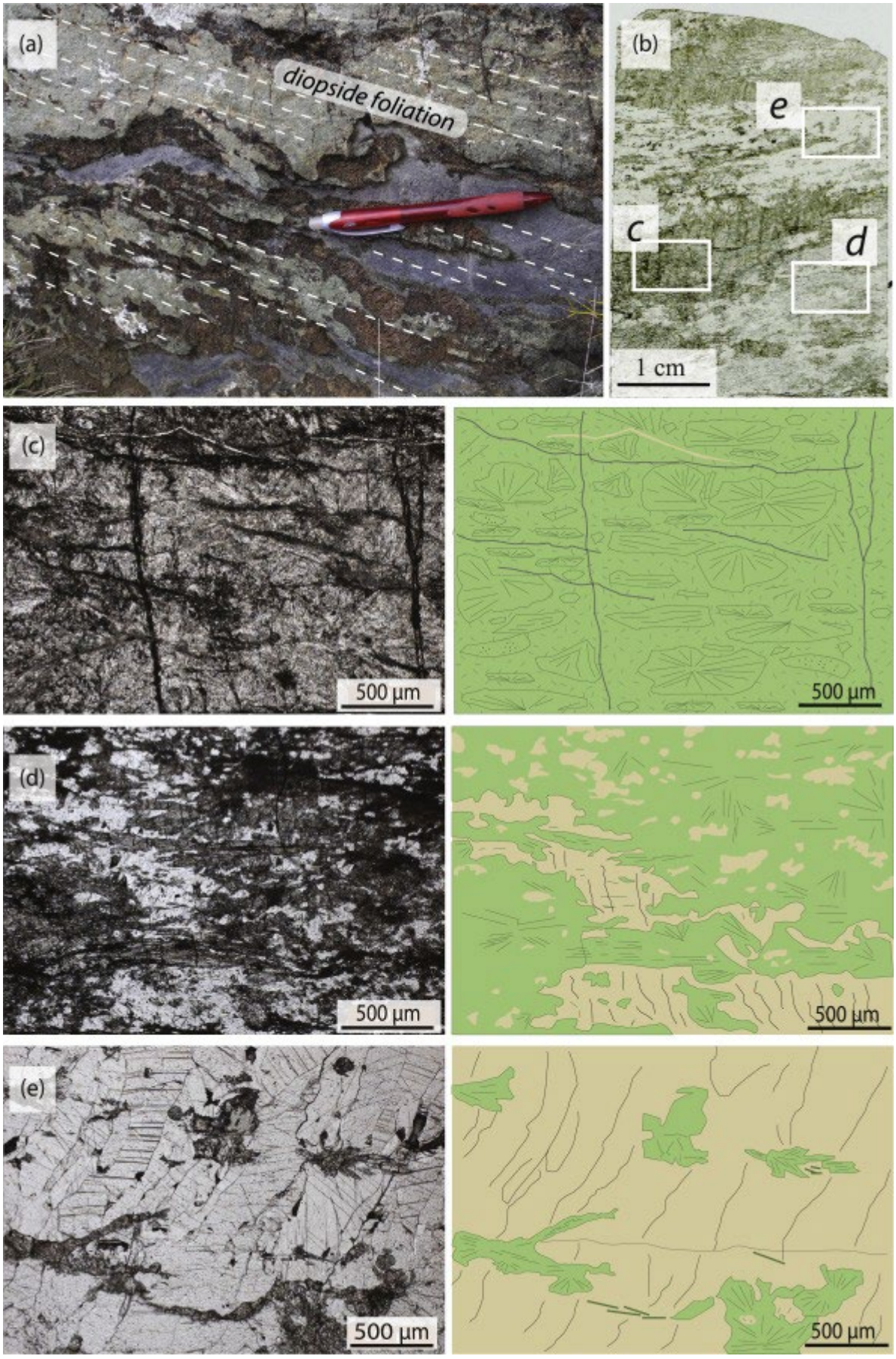

Fig. 4. Progressive transformation of a precursor Stage#1 carbonate-free, diopside-lawsonite rock into a Stage#2 metasomatic marble. a) Stage#2 metasomatic marble cropping out along the serpentinite-

metasediment contact. The marble (grey) is interdigitated with the host Stage#1 diopside-lawsonite rock (green). The foliation of the diopside-lawsonite rock (dashed line) can be followed in the carbonate layer. b) Thin section scan showing the interdigitation texture of silicate and carbonate layers analogous to that documented at the outcrop scale in part (a). Different degrees of carbonation are observed. White boxes indicate the location of the photomicrographs c, d and e. c) Plane polarized light photomicrograph and corresponding sketch of the preserved portion of the Stage#1 diopside-lawsonite rock; fan-shape diopside and lawsonite crystals statically crystallized. d) Plane polarized light photomicrograph and corresponding sketch of the patchy distribution of carbonate pods that characterizes a partially carbonated domain. Here, Stage#1 diopside aggregates are cut by the carbonate and some fragments are preserved as relicts in carbonate layers. e) Plane polarized light photomicrograph and corresponding sketch of a highly carbonated portion. Here the rock is transformed into a metasomatic marble; prismatic carbonate crystals are well developed. A few remnants of Stage#1 diopside are preserved; these relicts display embayed rims and atoll-like textures. In every sketch, Stage#1 diopside-lawsonite domains are represented in green, whereas rod-shaped carbonate is in light beige. (For interpretation of the references to color in this figure legend, the reader is referred to the web version of this article.)

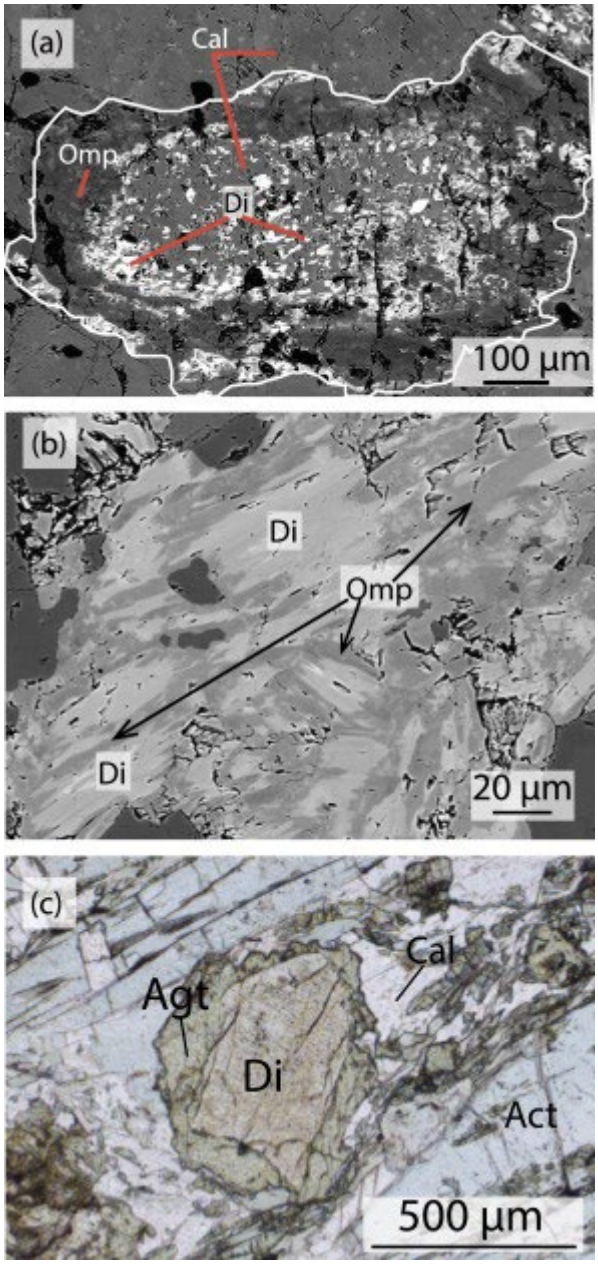

Fig. 5. Backscattered electron (BSE) images obtained by SEM and photomicrograph depicting micro-scale textural relationships resulting from fluid–rock interaction. a) BSE image of atoll-like Stage#1 diopside suggesting a digestion of silicates by carbonate; the Stage#1 diopsidic core is dissolved in favor of carbonate while a Stage#2 Na–Al rich rim (omphacite) crystallized in textural equilibrium with the carbonate. Small fragments of diopside are preserved as inclusions in carbonate crystals (red lines). b) BSE image of wallrock selvage shown in Fig. 3d. Diopside is overgrown by omphacite rim. Omphacite rims have the same composition of the vein infill omphacite crystals (Table S1). c) Plane polarized light photomicrograph of diopside with aegirine-augite rim in sample COR13-21d. Cal = calcite, Omp = omphacite, Di = diopside; Agt = aegirine-augite, Act = actinolite. (For interpretation of the references to color in this figure legend, the reader is referred to the web version of this article.)

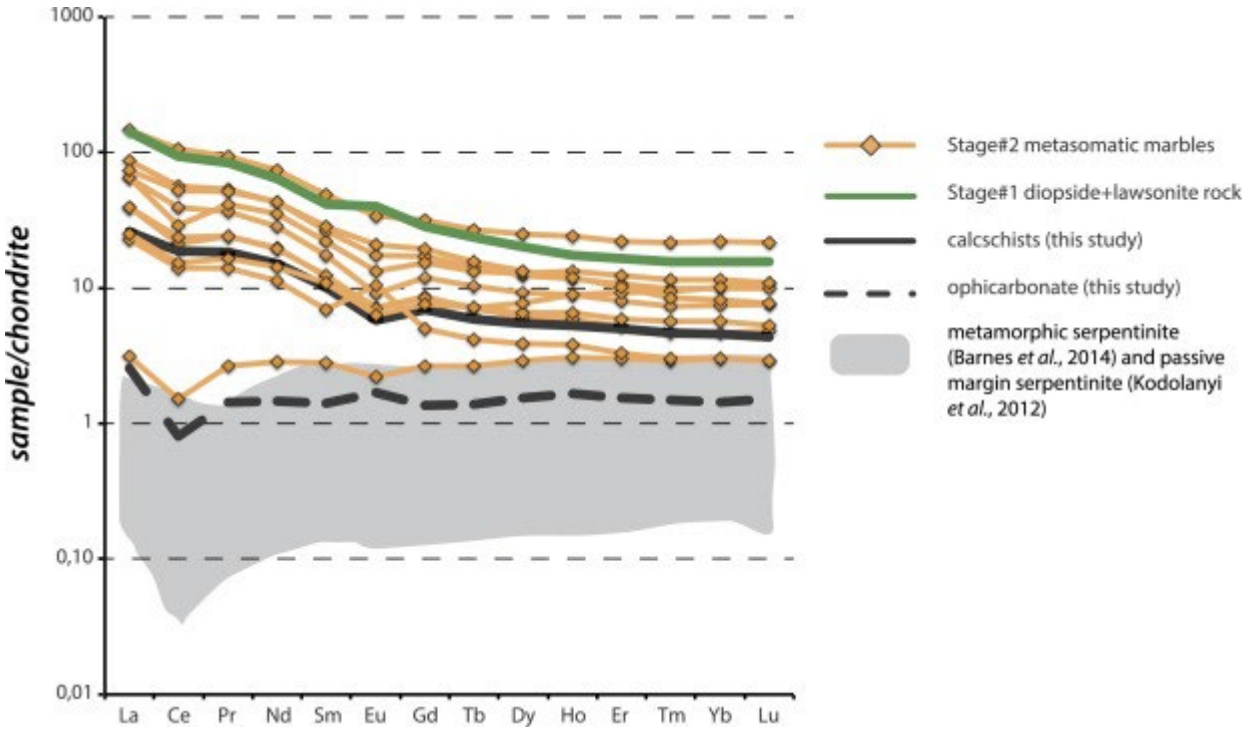

Fig. 6. Whole-rock chondrite normalized REE patterns (CI values from Sun and McDonough, 1989) for metasomatic marbles (orange lines, see Fig. S3 for details), reference calcschist and ophicarbonate (solid and dashed black lines, respectively), and Stage#1 diopside-lawsonite rock (solid green line). The shaded field represents the range of passive margin serpentinite whole-rock composition (either actual or metamorphic equivalent of Tethyan ocean floor; data from Barnes et al., 2014, Kodolányi et al., 2012). (For interpretation of the references to color in this figure legend, the reader is referred to the web version of this article.)

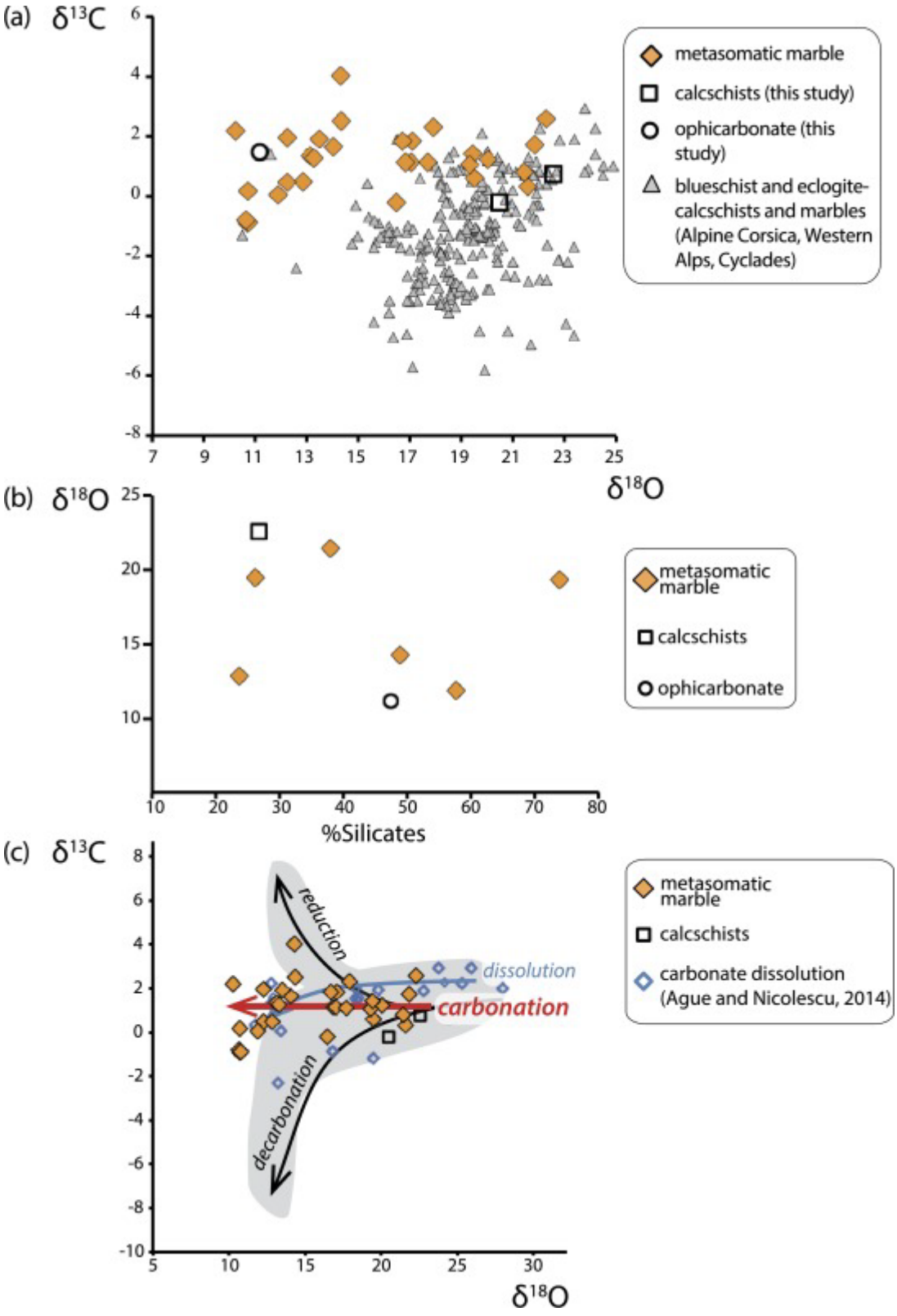

Fig. 7. Carbon and Oxygen stable isotopes analyses of calcite. a) Calcite $\delta^{13}C$ vs. $\delta^{18}O$ plot of metasomatic marbles (this study), blueschist and eclogite-facies marbles and calcite veins from other studies (Ague and Nicolescu, 2014, Cartwright and Buick, 2000, Cook-Kollars et al., 2014, Galvez et al., 2013b). Only data for non-metasomatic calcschists in Ague and Nicolescu (2014) and Galvez et al. (2013b) are reported. b) The rock silicate mineral content vs. calcite $\delta^{18}O$ values. The dispersion of data illustrates the lack of correlation between the light O isotopic signature and the silicate content. Analyses of reference calcschist and ophicarbonate are also reported. We plotted data for samples that were also analyzed for their bulk rock

composition (samples COR13-32; COR13-30a; COR13-21b; COR13-21d; COR13-27e; COR13-17c; COR13-22c; COR13-28c; Table S2). c) Metasomatic marble and reference calcschists $\delta^{18}O$ vs. $\delta^{13}C$ plot. Shaded areas correspond to geochemical trend of carbonate affected by devolatilization (Bowman et al., 2009; Gerdes et al., 1995, Gerdes et al., 1999), and carbonate reduction (Galvez et al., 2013b). Isotopic composition of carbonates affected by carbonate dissolution is also reported (blue diamonds, Ague and Nicolescu, 2014). (For interpretation of the references to color in this figure legend, the reader is referred to the web version of this article.)

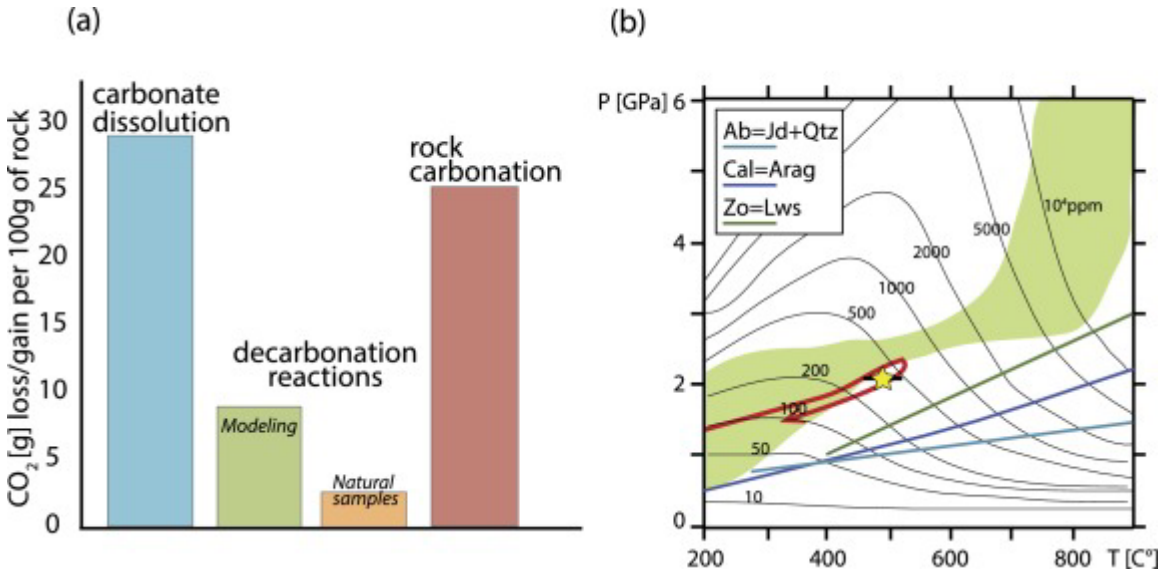

Fig. 8. Carbon fluxes during subduction metamorphism. a) Bar diagram reporting the estimation of grams of CO2 release per 100 g of precursor rock during carbonate dissolution (Ague and Nicolescu, 2014, blue bar) and decarbonation reactions (Cook-Kollars et al., 2014, calculation by Perple_X software and natural sample estimation, green and orange bars respectively) and grams of CO2 bound per 100 g of precursor rock via carbonate precipitation (red bar, this study). b) Contours of [C] in parts per million for aqueous fluid saturated in CaCO3 as a function of P and T. The red arrow indicates the P–T path of Alpine Corsica (Vitale Brovarone et al., 2011a). The star corresponds to the equilibrium temperature and the bar indicates temperature uncertainty. The green field represents the predicted P–T path for active subduction (D80 model, Syracuse et al., 2010). Figure adapted from Kelemen and Manning (2015). (For interpretation of the references to color in this figure legend, the reader is referred to the web version of this article.)

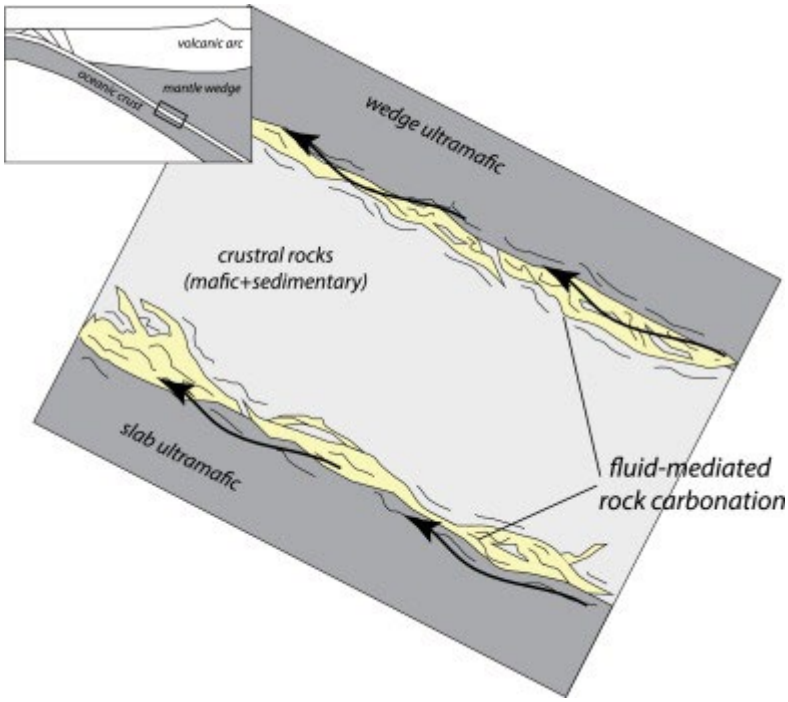

Fig. 9. Schematic illustration showing the percolation of COH fluids parallel to the subducting slab. The decreasing T and consequent decrease in carbonate solubility along this ascent path together with the interaction with slab or mantle rock is a suitable context for carbonate precipitation via vein injection and mineral carbonation.

References

J.J. Ague Fluid infiltration and transport of major, minor, and trace elements during regional Metamorphism of Carbonate Rocks, Wepawaug Schist, Connecticut, USA Am. J. Sci., 303 (2003), pp. 753-816

J.J. Ague, S. Nicolescu Carbon dioxide released from subduction zones by fluid-mediated reactions Nat. Geosci., 7 (2014), pp. 355-360

J.C. Alt, D.A.H. Teagle The uptake of carbon during alteration of ocean crust Geochim. Cosmochim. Acta, 63 (1999), pp. 1527-1535

S. Angiboust, T. Pettke, J.C.M. De Hoog, B. Caron, O. Oncken Channelized fluid flow and eclogite-facies metasomatism along the Subduction Shear Zone J. Petrol., 55 (2014), pp. 883-916

J.D. Barnes, M. Beltrando, C.-T.A. Lee, M. Cisneros, S. Loewy, E. Chin Geochemistry of Alpine serpentinites from rifting to subduction: a view across paleogeographic domains and metamorphic grade Chem. Geol., 389 (2014), pp. 29-47

G.E. Bebout, M.D. Barton Fluid flow and metasomatism in a subduction zone hydrothermal system: Catalina Schist terrane, California Geology, 17 (1989), pp. 976-980

M. Beltrando, G. Manatschal, G. Mohn, G.V. Dal Piaz, A. Vitale Brovarone, E. Masini Recognizing remnants of magma-poor rifted margins in high-pressure orogenic belts: the Alpine case study Earth-Sci. Rev., 131 (2014), pp. 88-115,

R.A. Berner, Z. Kothavala GEOCARB III: a revised model of atmospheric CO2 over Phanerozoic time Am. J. Sci., 301 (2001), pp. 182-204

T.M. Boundy, C.L. Donohue, E.J. Essene, K. Mezger, H. Austrheim Discovery of eclogite facies carbonate rocks from the Lindås Nappe, Caledonides, Western Norway J. Metamorph. Geol., 20 (2002), pp. 649-667

J.R. Bowman, J.W. Valley, N.T. Kita Mechanisms of oxygen isotopic exchange and isotopic evolution of 18O/16O-depleted periclase zone marbles in the Alta aureole, Utah: insights from ion microprobe analysis of calcite Contrib. Mineral. Petrol., 157 (2009), pp. 77-93,

J.B. Brady, M.J. Markley, J.C. Schumacher, J.T. Cheney, G.A. Bianciardi Aragonite pseudomorphs in high-pressure marbles of Syros, Greece J. Struct. Geol., 26 (2004), pp. 3-9

V. Busigny, P. Cartigny, P. Philippot, M. Ader, M. Javoy Massive recycling of nitrogen and other fluid-mobile elements (K, Rb, Cs, H) in a cold slab environment: evidence from HP to UHP oceanic metasediments of the Schistes Lustrés nappe (western Alps, Europe) Earth Planet. Sci. Lett., 215 (2003), pp. 27-42

N.C. Caciagli, C.E. Manning The solubility of calcite in water at 6–16 kbar and 500–800 °C Contrib. Mineral. Petrol., 146 (2003), pp. 275-285

J. Carignan, P. Hild, G. Mevelle, J. Morel, D. Yeghicheyan Routine analyses of trace elements in geological samples using flow injection and low pressure on-line liquid chromatography coupled to ICP-MS: a study of geochemical reference materials BR, DR-N, UB-N, AN-G and GH Geostand. Newsl., 25 (2001), pp. 187-198,

I. Cartwright, C.A. Barnicoat Stable isotope geochemistry of Alpine ophiolites: a window to ocean-floor hydrothermal alteration and constraints on fluid–rock interaction during high-pressure metamorphism Int. J. Earth Sci., 88 (1999), pp. 219-235,

I. Cartwright, I.S. Buick Fluid generation, vein formation and the degree of fluid–rock interaction during decompression of high-pressure terranes: the Schistes Lustrés, Alpine Corsica, France J. Metamorph. Geol., 18 (2000), pp. 607-624

J.A.D. Connolly Computation of phase equilibria by linear programming: a tool for geodynamic modeling and its application to subduction zone decarbonation Earth Planet. Sci. Lett., 236 (2005), pp. 524-541

J. Cook-Kollars, G.E. Bebout, N.C. Collins, S. Angiboust, P. Agard Subduction zone metamorphic pathway for deep carbon cycling: I. Evidence from HP/UHP metasedimentary rocks, Italian Alps Chem. Geol., 386 (2014), pp. 31-48,

F. Deschamps, M. Godard, S. Guillot, K. Hattori Geochemistry of subduction zone serpentinites: a review Lithos, 178 (2013), pp. 96-127,

M. Faccenda Water in the slab: a trilogy Tectonophysics, 614 (2014), pp. 1-30

S. Facq, I. Daniel, G. Montagnac, H. Cardon, D.A. Sverjensky In situ Raman study and thermodynamic model of aqueous carbonate speciation in equilibrium with aragonite under subduction zone conditions Geochim. Cosmochim. Acta, 132 (2014), pp. 375-390,

J. Fein, J. Walther Calcite solubility and speciation in supercritical NaCl–HCl aqueous fluids Contrib. Mineral. Petrol., 103 (1989), pp. 317-324,

M. Fournier, L. Jolivet, B. Goff, R. Dubois Alpine Corsica metamorphic core complex Tectonics, 10 (1991), pp. 1173-1186

M.L. Frezzotti, J. Selverstone, Z.D. Sharp, R. Compagnoni Carbonate dissolution during subduction revealed by diamond-bearing rocks from the Alps Nat. Geosci., 4 (2011), pp. 703-706

P. Fryer, J.A. Pearce, L.B. Stokking, et al. 36. A synthesis of Leg 125 drilling of serpentine seamounts on the Mariana and Izu–Bonin forearcs Proceedings of the Ocean Drilling Program, Scientific Results (1992), pp. 593-614

M.E. Galvez, O. Beyssac, I. Martinez, K. Benzerara, C. Chaduteau, B. Malvoisin, J. Malavieille Graphite formation by carbonate reduction during subduction Nat. Geosci., 6 (2013), pp. 473-477

M.E. Galvez, I. Martinez, O. Beyssac, K. Benzerara, P. Agrinier, N. Assayag Metasomatism and graphite formation at a lithological interface in Malaspina (Alpine Corsica, France) Contrib. Mineral. Petrol., 166 (2013), pp. 1687-1708

M.L. Gerdes, L.P. Baumgartner, M. Person, D. Rumble One-and two-dimensional models of fluid flow and stable isotope exchange at an outcrop in the Adamello contact aureole, Southern Alps, Italy Am. Mineral., 80 (1995), pp. 1004-1019

M.L. Gerdes, L.P. Baumgartner, J.W. Valley Stable isotopic evidence for limited fluid flow through dolomitic marble in the Adamello contact aureole, Cima Uzza, Italy J. Petrol., 40 (1999), pp. 853-872

P.J. Gorman, D.M. Kerrick, J.A.D. Connolly Modeling open system metamorphic decarbonation of subducting slabs: metamorphic decarbonation Geochem. Geophys. Geosyst., 7 (2006)

F. Guyot, D. Daval, S. Dupraz, I. Martinez, B. Ménez, O. Sissmann CO2 geological storage: the environmental mineralogy perspective C. R. Geosci., 343 (2011), pp. 246-259

J. Hoefs Stable Isotope Geochemistry Springer Science & Business Media (2013)

R. Hoffbauer, S. Hoernes, E. Fiorentini Oxygen isotope thermometry based on a refined increment method and its application to granulite-grade rocks from Sri Lanka Precambrian Res., 66 (1994), pp. 199-220

M. Jébrak Hydrothermal breccias in vein-type ore deposits: a review of mechanisms, morphology and size distribution Ore Geol. Rev., 12 (1997), pp. 111-134

L. Jolivet, J.-M. Daniel, M. Fournier Geometry and kinematics of extension in Alpine Corsica Earth Planet. Sci. Lett., 104 (1991), pp. 278-291

L. Jolivet, R. Dubois, M. Fournier, B. Goffé, A. Michard, C. Jourdan Ductile extension in alpine Corsica Geology, 18 (1990), pp. 1007-1010,

P.B. Kelemen, C.E. Manning Reevaluating carbon fluxes in subduction zones, what goes down, mostly comes up Proc. Natl. Acad. Sci. USA, 112 (30) (2015), pp. E3997-E4006,

D.M. Kerrick, J.A.D. Connolly Metamorphic devolatilization of subducted marine sediments and the transport of volatiles into the Earth's mantle Nature, 411 (2001), pp. 293-296

B.I. Kleine, A.D.L. Skelton, B. Huet, I.K. Pitcairn Preservation of blueschist-facies minerals along a shear zone by coupled metasomatism and fast-flowing CO2-bearing fluids J. Petrol., 55 (2014), pp. 1905-1939,

J. Kodolányi, T. Pettke, C. Spandler, B.S. Kamber, K. Gmeling Geochemistry of ocean floor and fore-arc serpentinites: constraints on the ultramafic input to subduction zones J. Petrol., 53 (2012), pp. 235-270

C. Lazar, C. Zhang, C.E. Manning, B.O. Mysen Redox effects on calcite–portlandite–fluid equilibria at forearc conditions: carbon mobility, methanogenesis, and reduction melting of calcite Am. Mineral., 99 (2014), pp. 1604-1615

Malavieille, Chemenda, Larroque Evolutionary model for Alpine Corsica: mechanism for ophiolite emplacement and exhumation of high-pressure rocks Terra Nova, 10 (1998), pp. 317-322,

B. Malvoisin, C. Chopin, F. Brunet, M.E. Galvez Low-temperature wollastonite formed by carbonate reduction: a marker of serpentinite redox conditions J. Petrol., 53 (2012), pp. 159-176,

C.E. Manning, E.L. Shock, D.A. Sverjensky The chemistry of carbon in aqueous fluids at crustal and upper-mantle conditions: experimental and theoretical constraints Rev. Mineral. Geochem., 75 (2013), pp. 109-148

L.A.J. Martin, D. Rubatto, C. Crépisson, J. Hermann, B. Putlitz, A. Vitale-Brovarone Garnet oxygen analysis by SHRIMP-SI: matrix corrections and application to high-pressure metasomatic rocks from Alpine Corsica Chem. Geol., 374–375 (2014), pp. 25-36,

L.A.J. Martin, D. Rubatto, A. Vitale Brovarone, J. Hermann Late Eocene lawsonite-eclogite facies metasomatism of a granulite sliver associated to ophiolites in Alpine Corsica Lithos, 125 (2011), pp. 620-640,

J.M. Matter, P.B. Kelemen Permanent storage of carbon dioxide in geological reservoirs by mineral carbonation Nat. Geosci., 2 (2009), pp. 837-841

J.M. McCrea On the isotopic chemistry of carbonates and a paleotemperature scale J. Chem. Phys., 18 (1950), p. 849

J.A. Miller, I. Cartwright, I.S. Buick, A.C. Barnicoat An O-isotope profile through the HP–LT Corsican ophiolite, France and its implications for fluid flow during subduction Chem. Geol., 178 (2001), pp. 43-69

J.F. Molina, S. Poli Carbonate stability and fluid composition in subducted oceanic crust: an experimental study on H2O–CO2-bearing basalts Earth Planet. Sci. Lett., 176 (2000), pp. 295-310

G. Molli, J. Malavieille Orogenic processes and the Corsica/Apennines geodynamic evolution: insights from Taiwan Int. J. Earth Sci. (Geol. Rundsch.), 100 (2011), pp. 1207-1224,

N. Morimoto Nomenclature of pyroxenes Mineral. Petrol., 39 (1988), pp. 55-76,

R.C. Newton, C.E. Manning Experimental determination of calcite solubility in H2O–NaCl solutions at deep crust/upper mantle pressures and temperatures: implications for metasomatic processes in shear zones Am. Mineral., 87 (2002), pp. 1401-1409

T. Nishiyama CO2-metasomatism of a metabasite block in a serpentine melange from the Nishisonogi metamorphic rocks, southwest Japan Contrib. Mineral. Petrol., 104 (1990), pp. 35-46

K.-H. Nitsch The P–T–XCO2 Stabilitätsfeld von Lawsonit Contrib. Mineral. Petrol., 34 (1972), pp. 116-134

T. Plank, C.H. Langmuir The chemical composition of subducting sediment and its consequences for the crust and mantle Chem. Geol., 145 (1998), pp. 325-394

S. Poli Carbon mobilized at shallow depths in subduction zones by carbonatitic liquids Nat. Geosci., 8 (2015), pp. 633-636

S. Poli, E. Franzolin, P. Fumagalli, A. Crottini The transport of carbon and hydrogen in subducted oceanic crust: an experimental study to 5 GPa Earth Planet. Sci. Lett., 278 (2009), pp. 350-360

A. Putnis, T. John Replacement processes in the Earth's crust Elements, 6 (2010), pp. 159-164

E.J.K. Ravna, T.B. Andersen, L. Jolivet, C. De Capitani Cold subduction and the formation of lawsonite eclogite – constraints from prograde evolution of eclogitized pillow lava from Corsica J. Metamorph. Geol., 28 (2010), pp. 381-395

D. Rumble III, J. Farquhar, E.D. Young, C.P. Christensen In situ oxygen isotope analysis with an excimer laser using F2 and BrF5 reagents and O2 gas as analyte Geochim. Cosmochim. Acta, 61 (1997), pp. 4229-4234

N.C.A. Seaton, D.L. Whitney, C. Teyssier, E. Toraman, M.T. Heizler Recrystallization of high-pressure marble (Sivrihisar, Turkey) Tectonophysics, 479 (2009), pp. 241-253

S. Sun, W.F. McDonough Chemical and isotopic systematics of oceanic basalts: implications for mantle composition and processes Geol. Soc. (Lond.) Spec. Publ., 42 (1989), pp. 313-345

D.A. Sverjensky, V. Stagno, F. Huang Important role for organic carbon in subduction-zone fluids in the deep carbon cycle Nat. Geosci., 7 (2014), pp. 909-913

E.M. Syracuse, P.E. van Keken, G.A. Abers The global range of subduction zone thermal models Phys. Earth Planet. Inter., 183 (2010), pp. 73-90

J.W. Valley Stable isotope geochemistry of metamorphic rocks Rev. Mineral. Geochem., 16 (1986), pp. 445-489

A. Vitale Brovarone, O. Alard, O. Beyssac, L. Martin, M. Picatto Lawsonite metasomatism and trace element recycling in subduction zones J. Metamorph. Geol., 32 (2014), pp. 489-514

A. Vitale Brovarone, M. Beltrando, J. Malavieille, F. Giuntoli, E. Tondella, C. Groppo, O. Beyssac, R. Compagnoni Inherited Ocean–Continent Transition zones in deeply subducted terranes: insights from Alpine Corsica Lithos, 124 (2011), pp. 273-290

A. Vitale Brovarone, O. Beyssac Lawsonite metasomatism: a new route for water to the deep Earth Earth Planet. Sci. Lett., 393 (2014), pp. 275-284

A. Vitale Brovarone, O. Beyssac, J. Malavieille, G. Molli, M. Beltrando, R. Compagnoni Stacking and metamorphism of continuous segments of subducted lithosphere in a high-pressure wedge: the example of Alpine Corsica (France) Earth-Sci. Rev., 116 (2013), pp. 35-56,

A. Vitale Brovarone, C. Groppo, G. Hetényi, R. Compagnoni, J. Malavieille Coexistence of lawsonite-bearing eclogite and blueschist: phase equilibria modelling of Alpine Corsica metabasalts and petrological evolution of subducting slabs J. Metamorph. Geol., 29 (2011), pp. 583-600

A. Vitale Brovarone, D. Herwartz Timing of HP metamorphism in the Schistes Lustrés of Alpine Corsica: new Lu–Hf garnet and lawsonite ages Lithos, 172–173 (2013), pp. 175-191

J.V. Walther, M.I. Long Experimental determination of calcite solubilities in supercritical H2O Int. Symp. Water–Rock Interaction, vol. 5 (1986), pp. 609-611

Q. Wang, D. Rumble Oxygen and carbon isotope composition from the UHP Shuanghe marbles, Dabie Mountains, China Sci. China, Ser. D, Earth Sci., 42 (1999), pp. 88-96

C.R. Wilson, M. Spiegelman, P.E. van Keken, B.R. Hacker Fluid flow in subduction zones: the role of solid rheology and compaction pressure Earth Planet. Sci. Lett., 401 (2014), pp. 261-274

Y.-F. Zheng Calculation of oxygen isotope fractionation in anhydrous silicate minerals Geochim. Cosmochim. Acta, 57 (1993), pp. 1079-1091

Y.F. Zheng Oxygen isotope fractionation in metal monoxides Mineral. Mag. A, 58 (1994), pp. 1000-1001